Mathematical Biosciences and Engineering

MBE, 19(1): 688−706.
DOI: 10.3934/mbe.2022031
Received: 08 August 2021
Accepted: 07 November 2021
Published: 19 November 2021

http://www.aimspress.com/journal/MBE

Research article

Construction and validation of a novel pyroptosis-related signature to predict prognosis in patients with cutaneous melanoma

Zehao Niu[1,2,†], Yujian Xu[2,†], Yan Li[1,2,†], Youbai Chen[2,*] and Yan Han[2,*]

[1] Medical School of Chinese PLA, Beijing 100853, China
[2] Department of Plastic and Reconstructive Surgery, the First Medical Center, Chinese PLA General Hospital, Beijing 100853, China

* **Correspondence:** Email: 13720086335@163.com, chenyoubai@301hospital.com.cn.

† These authors contributed equally to this work.

Abstract: Skin cutaneous melanoma (SKCM) is one of the most malignant skin cancers and remains a health concern worldwide. Pyroptosis is a newly recognized form of programmed cell death and plays a vital role in cancer progression. We aim to construct a prognostic model for SKCM patients based on pyroptosis-related genes (PRGs). SKCM patients from The Cancer Genome Atlas (TCGA) were divided into training and validation cohorts. We used GSE65904 downloaded from GEO database as an external validation cohort. We performed Cox regression and the least absolute shrinkage and selection operator (LASSO) regression to identify prognostic genes and built a risk score. Patients were divided into high- and low-risk groups based on the risk score. Differently expressed genes (DEGs), immune cell infiltration and immune-related pathways activation were compared between the two groups. We established a model containing 4 PRGs, i.e., GSDMA, GSDMC, AIM2 and NOD2. The overall survival (OS) time was significantly different between the 2 groups. The risk score was an independent predictor for prognosis in both the uni- and multi-variable Cox regressions. Gene ontology (GO) and Kyoto Encylopedia of Genes and Genomes (KEGG) analyses showed that DEGs were enriched in immune-related pathways. Most types of immune cells were highly expressed in the low-risk group. All immune pathways were significantly up-regulated in the low-risk group. In addition, low-risk patients had a better response to immune checkpoint inhibitors. Our novel pyroptosis-related gene signature could predict the prognosis of SKCM patients and their response to immune checkpoint inhibitors.

Keywords: melanoma; TCGA; prognostic prediction; treatment; biomarkers

1. Introduction

Skin cutaneous melanoma (SKCM) is the most malignant cutaneous tumor and accounts for the majority of skin cancer-related deaths [1]. According to the 2019 cancer treatment and survivorship statistics [2], SKCM is one of the top five prevalent cancers (684,470 cases among males and 672,140 cases among females). Early stage SKCM is curable with extended resection treatment [3]. However, a large number of high-risk SKCM patients develop metastasis and have poor prognosis. For patients diagnosed with metastatic SKCM, the 5-year survival probability is only 19% [2−4]. However, it is difficult to identify high-risk patients and intervene accordingly. Thus, it is urgent to build a reliable prognostic model to predict patients' survival.

Pyroptosis, a form of programmed cell death (PCD) [5], is characterized by consecutive cell expansion until membrane breaks down and cell contents leakage, leading to the activation of intense immune response [6]. Recent studies showed that some key pyroptosis mediators, such as Gasdermin (GSDM) family [7], NOD-like receptor (NLRs) family [8] and cysteinyl aspartate protease (CASP) family [9], are dysfunctional in multiple cancers. For example, Wei et al. [10] noted that NLRP3 was downregulated or even completely absent in hepatocellular carcinoma. Hergueta et al. [11] reported that GSDMB was associated with invasion and metastasis in breast cancer cells. Wang et al. [12] found that GSDMD could promote gastric cancer proliferation and regulate cell cycle-related proteins. Ye et al. [13] summarized pyroptosis-related genes (PRGs) and constructed a novel model for predicting the prognosis of ovarian cancer.

The role of pyroptosis in the development and progression of SKCM has also been investigated. For example, Dan et al. [14] reported that combined use of BRAFi and MEKi targeted therapies promoted cleavage of GSDME and induced pyroptosis in SKCM. Moreover, Zhou et al. [15] reported that iron-activated ROS signaling could cleave GSDME and promote melanoma cell pyroptosis. Combination of iron and ROS-inducing drugs could inhibit SKCM growth by activating GSDME-dependent pyroptosis. However, the predictive ability of PRGs for the survival of CM patients has not been elucidated. Thus, this study was intended to construct a PRG signature to predict the prognosis of SKCM patients and their response to immunotherapy.

2. Materials and methods

The flow chart of this study is shown in Figure 1.

2.1. Data resources and normalization

Due to the lack of normal samples in TCGA dataset, GTEx dataset was used as normal control. GTEx datasets (FPKM, $\log_2(x+0.001)$ transformed) were downloaded from the University of California Santa Cruz (UCSC) Xena website (https://xenabrowser.net/datapages/) on 20 February 2021. Gene expression data of TCGA-SKCM (FPKM) and corresponding clinical features were downloaded from TCGA database (https://portal.gdc.cancer.gov/repository). Patients with incomplete clinical data or follow-up time < 90 days were deleted. The gene expression data from TCGA database were $\log_2(x+0.001)$ transformed and merged with gene expression data from GTEx database using "limma"

package in R software (v4.0.3). In total, 443 patients (all from TCGA dataset) and 813 normal controls (all from GTEx dataset, including not sun exposed skin from suprapubic and sun exposed skin from lower leg) were included in this study. Then, 443 patients in the tumor group were randomly divided into the training cohort and validation cohort at a ratio of 7:3. Specifically, 311 patients were set as the training cohort and 132 patients were set as the validation cohort. Subsequently, GSE65904 containing 214 patients was downloaded from GEO (Gene Expression Omnibus, https://www.ncbi.nlm.nih.gov/geo/) as an external validation cohort.

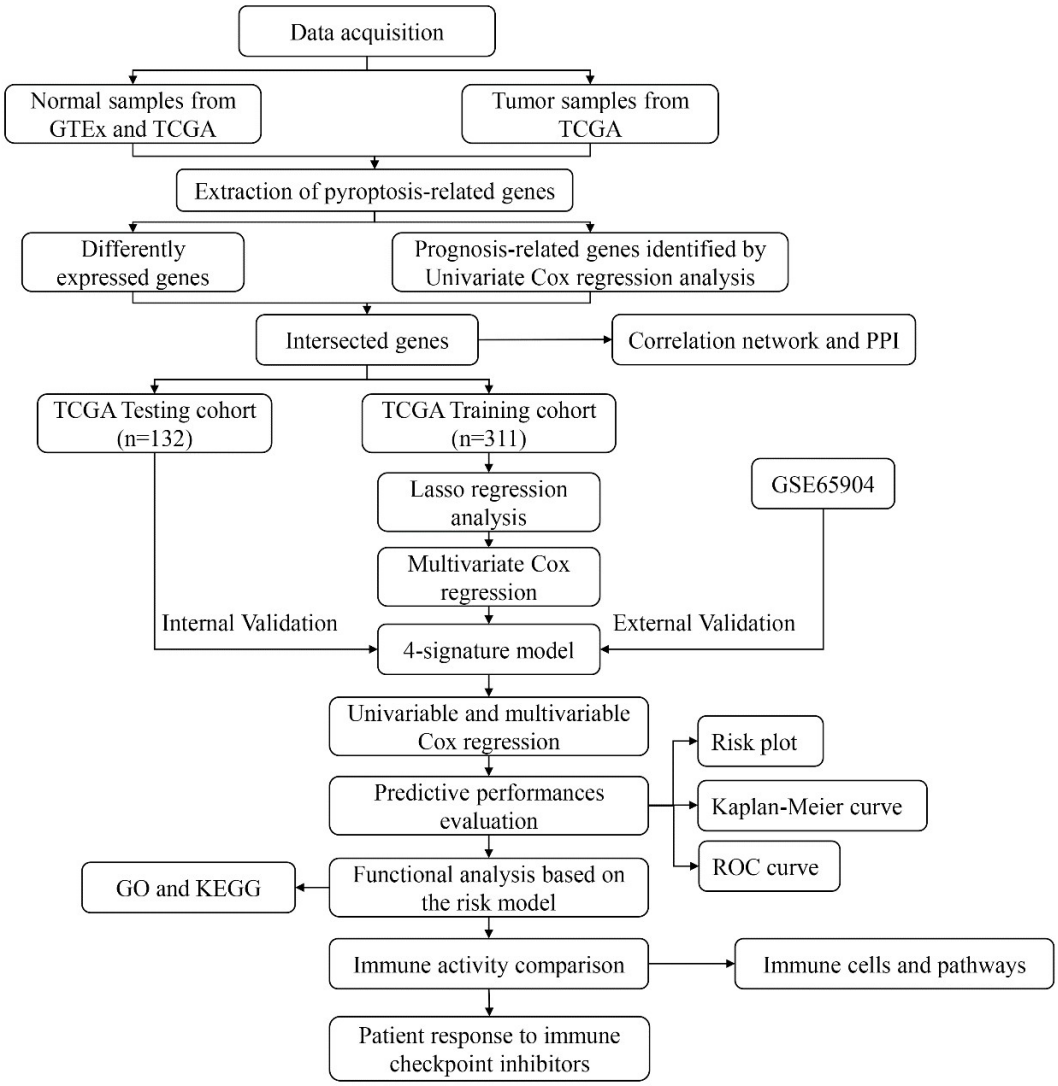

Figure 1. Workflow diagram for analyzing pyroptosis-related genes in SKCM.

2.2. Identification of differently expressed pyroptosis-related genes

PRGs were extracted according to previous studies [13]. Differently expressed genes (DEGs) between the cancer group and normal control were identified using the "limma" package. P value < 0.05 and $Log_2(|\text{fold change}|) > 0.586$ was considered the cut-off.

2.3. Identification of prognosis-related genes

To explore the prognostic value of these PRGs, Cox regression analysis was conducted. Survival time and survival states were merged with mRNA expression data. *P* value < 0.05 was considered the cut-off. Prognosis-related genes were intersected with DEGs for further analysis. The protein-protein interaction (PPI) network was constructed and visualized using online tool at (https://string-db.org/). The correlation network of these intersected genes was constructed using the "igraph" package in R software.

2.4. Construction and evaluation of a prognostic model

The LASSO regression analysis was performed to eliminate genes that might overfit the model. In the training cohort, LASSO analysis was conducted by using the "glmnet" package in R software. The best penalty parameter lambda was chosen based on 10 cross-validation. Then, a multivariate Cox regression was performed to evaluate the contribution of each gene to prognosis prediction [16,17]. Finally, an algorithm for the risk score was established. The risk score was generated with a normalized expression value multiplied by corresponding regression coefficients (β). Each patient was assigned to a low-risk or high-risk group according to the median risk score. Overall survival (OS) time difference between the two groups was studied using Kaplan-Meier analysis. The receiver operating characteristic curve (ROC) and the area under the curve (AUC) were drawn using "survival", "survminer" and "timeROC" packages. Clinical data were combined with each patient' risk score. The correlations between the risk score and clinical features, such as T, N, M stage and age, were evaluated and visualized using "limma" and "ggpubr" packages. For internal validation studies, risk scores in the TCGA validation cohort was calculated using the same formula. Patients were divided into the low-risk and high-risk group before Kaplan-Meier analysis and the ROC curve were also used to assess the prognostic value of the model. For external validation, GSE65904 downloaded from GEO database was used as an external validation cohort. Expression profiles of each gene were normalized using the "sva" package in R. Risk score of each patient was calculated according to the formula of the model. Finally, training and testing cohorts from TCGA dataset were merged. The signature was validated in the entire cohort. A ROC curve, including clinical characteristics, was constructed, and the AUC was compared with the signature.

2.5. Independent prognostic value of the model

Univariate and multivariable Cox regression analyses were used to find out whether the risk score could serve as an independent prognostic factor. Clinical data, including age, gender, stage, T, M, N, were analyzed in combination with the risk score in both training and validation groups.

2.6. Function and pathway enrichment analysis of the DEGs

We further explored the DEGs between low- and high- risk groups in TCGA training cohort. $Log_2(|\text{fold change}|) \geq 1$ and FDR < 0.05 were considered the cutoff. GO function enrichment and KEGG pathway enrichment analysis were performed using "clusterProfiler" package. As indicated by previous literature, pyroptosis has some connections with immune response. Thus, we continued to

calculate the scores of infiltrating immune cells and evaluate the activity of immune-related pathways by using the "gsva" package in R software.

2.7. Patient response to immune checkpoint inhibitors and evaluation of checkpoint molecules

Given that immune therapy is currently widely used for melanoma patients, we evaluated patients' response to anti-cytotoxic T lymphocyte antigen-4 (CTLA-4) and anti-programmed cell death protein 1 (anti-PD-1) antibodies by immunophenoscore. The immunophenoscore (obtained from https://tcia.at/) was developed by Charoentong et al. [18] and has been proven to be a superior predictor of response to immune therapies. Expressions of checkpoint molecules, including PD-1, PD-L1, PD-L2 and CTLA-4 were analyzed.

2.8. Statistical analysis

R (v 4.0.3) was used in statistical analysis. The expression difference between melanoma and normal samples was compared using single-factor analysis of variance. Kaplan-Meier method was used to compare the overall survival time between high and low risk patients. The univariate and multivariate Cox regression model was used to access the independent prognostic value of the model.

3. Results

3.1. Identification of differently expressed pyroptosis-related genes

All pyroptosis-related genes were expressed differently between normal and tumor samples with P value < 0.05. Among them, 24 genes with Log2(|fold change|) ≥ 0.586 (fold change ≥ 1.5) were qualified for further studies. As shown in Figure 2A, 14 genes (ELANE, GSDMC, NLRP1, IL18, GSDMB, GSDMA, IL6, NOD2, PJVK, CASP4, NOD1, SCAF11, NLRP2, PLCG1) were downregulated, while 10 genes (CASP9, TNF, CASP3, IL1B, NLRP3, CASP5, NLRP6, NLRC4, NLRP7, AIM2) were up-regulated.

3.2. Identification of prognostic pyroptosis-related genes

As shown in the forest plot (Figure 2B), in univariate Cox regression analysis, 9 genes were risk factors (HR > 1) while the others were protective factors (HR < 1). Among them, 16 genes met the preset threshold (P value < 0.05) and were included into further studies. A total of 14 intersected genes were qualified for further study (Figure 2C). PPI analysis and correlation network of these intersected genes are shown in Figure 2D and E. The PPI network revealed the potential connection between these intersected genes. The PPI network contained 14 nodes and 49 edges, with an average node degree of 7 (Figure. 2D). More degree of proteins interacted with each other indicated more critical roles. Among them, IL18 (11 interactions), AIM2 (10 interactions), CASP5 (10 interactions) and NLPR4 (10 interactions) were at the center of the network, indicating these genes may play an important role in cutaneous melanoma. Correlation network revealed the similar findings (Figure 2E).

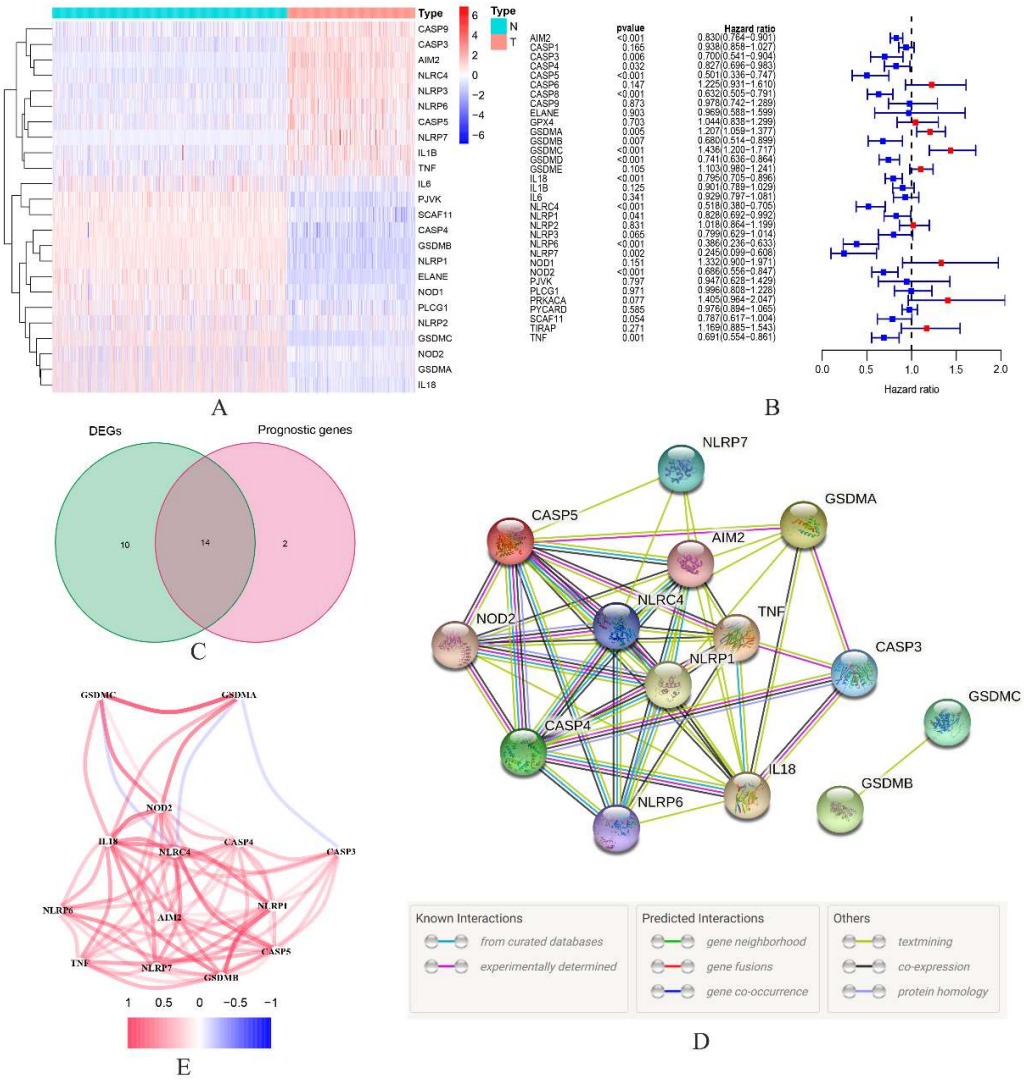

Figure 2. A. Heatmap of the differentially expressed pyroptosis-related genes in SKCM; B. Univariate cox regression analysis of each pyroptosis-related gene in SKCM, and 16 genes with $P < 0.05$; C. 24 DEGs and 16 genes with $P < 0.05$ in univariate cox regression analysis were intersected, and 14 intersected genes were included for further studies; D. PPI network of the interacted genes (intersected score = 0.4 medium confidence); E. The correlation network of the pyroptosis-related genes. (red line represents positive correlation and blue line represents negative correlation)

3.3. Construction of a prognostic model in the training cohort

After primary filtration, LASSO regression analysis was used to further narrow down the genes that may be put into the prognostic model. As shown in Figure 3A,B, eight genes (AIM2, CASP3, CASP5, GSDMA, GSDMC, IL18, NLRP6, NOD2) were identified according to the optimal lambda. Then, a stepwise multivariate Cox regression analysis was performed. Finally, a four-gene (GSDMA, GSDMC, AIM2, NOD2) signature was finally selected to construct a prognostic model. The risk score was calculated using the following formula: risk score = (0.038 × GSDMA exp.) + (0.310 × GSDMC exp.) + (−0.028 × AIM2 exp.) + (−0.437 × NOD2 exp.). According to the calculated risk

score, patients in the training group were divided into the high-risk group (n = 155) and low-risk groups (n = 156) (Figure 3C). As shown in Figure 3D, more patients in the high-risk group were clustered at the bottom of the scatter diagram, which meant they had a shorter survival time. In the survival curve (Figure 3E), there were more deaths in the high-risk group than in the low-risk group. The prognostic capacity of the model was assessed by calculating the AUC of the ROC curve. It was found that the AUCs of the model were 0.680,0.664 and 0.669 for 2-year, 3-year and 5-year survival (Figure 3F) respectively. In cox regression analyses (Figure 3G,H), the risk score had a significant relationship with OS both in univariate Cox regression and multivariate Cox regression. (HR = 1.083, 95% CI = 1.045−1.122, $P < 0.001$; HR = 1.082, 95% CI = 1.043−1.122, $P < 0.001$).

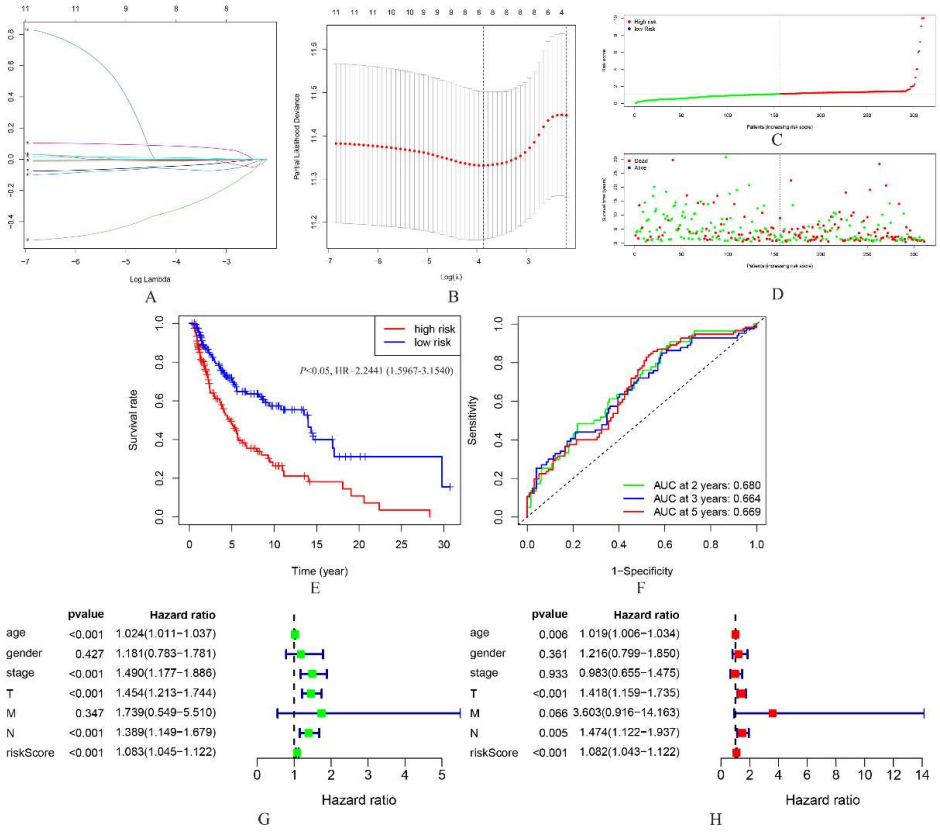

Figure 3. A,B. Determination of the number of factors by the LASSO analysis; C,D. distribution of patients based on the risk score in training cohort; E. Kaplan-Meier curves of patients in the high- and low-risk groups in training cohort. F. ROC corves of and area under the curve of risk score at 2, 3, 5 years for overall survival in training cohort. G,H. Univariate cox regression and multivariate cox regression in training cohort.

3.4. Validation of the prognostic model in the validation cohort

A total of 132 patients from TCGA dataset were set as the internal validation cohort, whose risk scores were calculated by using the same formula that was obtained from the training cohort and divided into the high-risk group (n = 62) and low-risk group (n = 62) (Figure 4A). Similarly, patients in the high-risk group had a much worse prognosis (Figure 4B,C). In addition, the AUC values were 0.703, 0.635 and 0.661 for 2-year, 3-year and 5-year survival (Figure 4D) respectively. In univariate

and multivariate Cox regression analysis (Figure 4E,F), the risk score could serve as an independent prognostic factor after adjusting for confounding factors (HR = 1.393 95% CI = 1.157−1.676, P < 0.001; HR = 1.252, 95% CI=1.023−1.533, P < 0.05 respectively). GSE65904 was set as the external validation cohort. Patients were divided into low-risk and high-risk groups based on the calculated risk scores (Figure 4G). The OS in the high-risk group was significantly poorer than it in the low-risk group (Figure 4H,I). AUC values from the ROC curves were 0.627, 0.649 and 0.622 for two, three, and five years, respectively. Then, TCGA training and testing cohorts were merged, the signature was validated in the entire cohort. Similar results were shown in Figures 5A-F. Specifically, the AUC values were 0.682, 0.665 and 0.673 for 2-year, 3-year and 5-year survival. These results indicated that the risk score could serve as an independent prognostic factor for melanoma patients.

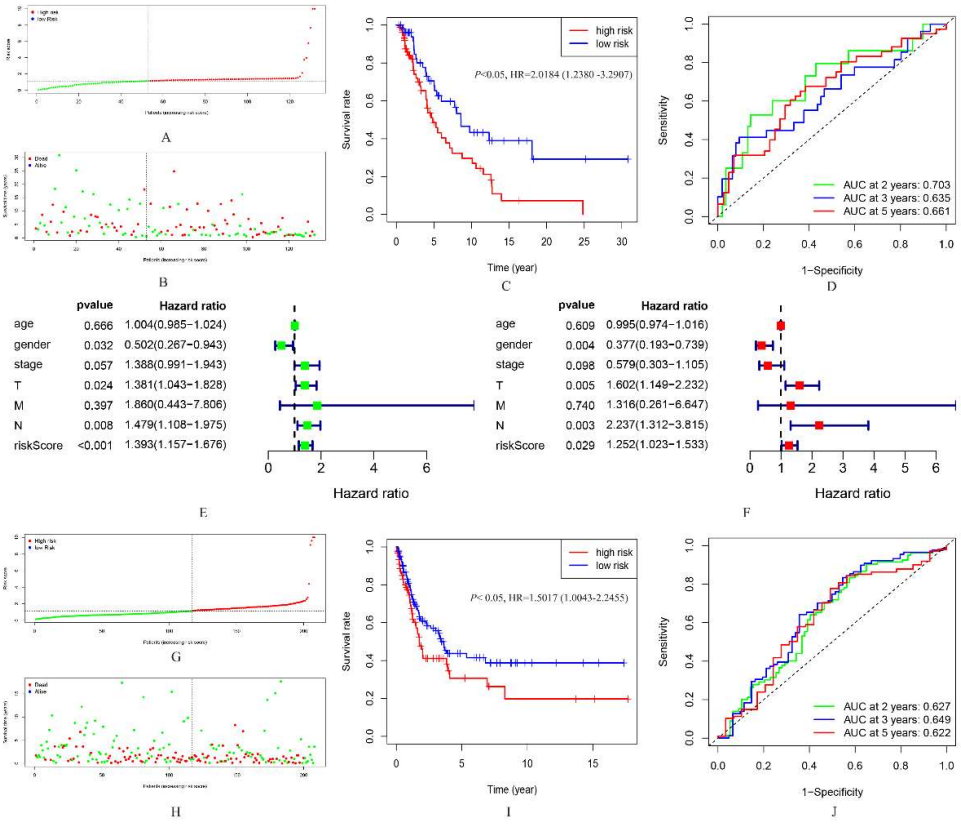

Figure 4. A, B. distribution of patients based on the risk score in internal validation cohort; C. Kaplan-Meier curves of patients in the high- and low-risk groups in internal validation cohort; D. ROC corves of and area under the curve of risk score at 2, 3, 5 years for overall survival in internal validation cohort; E, F. Univariate cox regression and multivariate cox regression in validation cohort; G, H. distribution of patients based on the risk score in external validation cohort; I. Kaplan-Meier curves of patients in the high- and low-risk groups in external validation cohort; J. ROC corves of and area under the curve of risk score at 2, 3, 5 years for overall survival in external validation cohort.

A ROC curve of clinicopathological features (age, gender, stage, TMN stage) was shown in Figure 5G. The AUC of risk core was higher than the AUC of age (0.523), gender (0.528), stage (0.671), T (0.690) and M stage (0.517), and was very close to the AUC of N stage (0.701). As shown in Figure 5H,

combined these clinical factors with the risk score could improve the AUC of prediction model to over 0.75. Specifically, a prediction model including risk score, T, and N was 0.794, indicating that the novel risk score significantly increased the predictive accuracy.

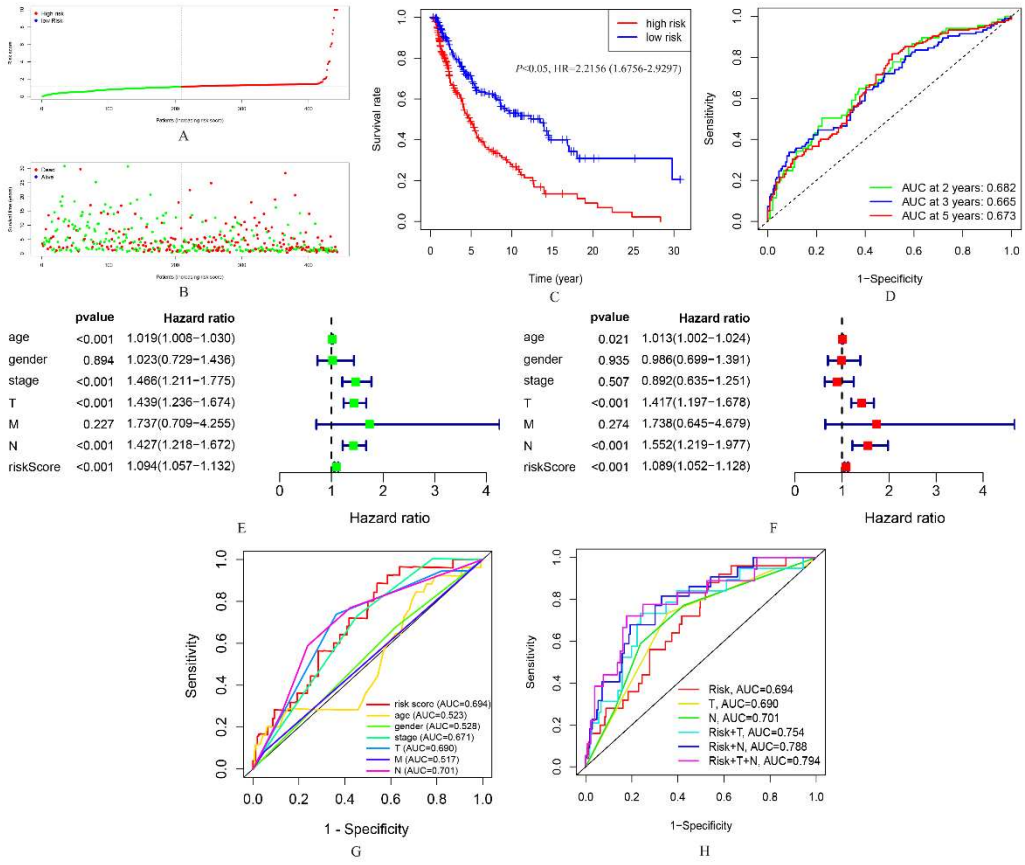

Figure 5. A, B. distribution of patients based on the risk score in the entire TCGA cohort; C. Kaplan-Meier curves of patients in the entire TCGA cohort; D. ROC corves of and area under the curve of risk score at 2, 3, 5 years for overall survival in the entire TCGA cohort; E, F. Univariate cox regression and multivariate cox regression in the entire TCGA cohort; G, H. ROC curve analysis of clinicopathological features.

3.5. Functional analyses based on the risk model

GO analysis and KEGG analysis were implemented based on the DEGs between high-risk and low-risk groups. In total, 1049 genes were identified by the preset criteria. Among them, 928 genes were down-regulated while 121 genes were up-regulated in the low-risk group. As shown in Figure 6A, the BP terms were mainly enriched in immune-related pathways, such as immune response-activating cell surface receptor signaling pathway and immune response-activating signal transduction. The CC term was mainly enriched on the external side of plasma membrane, immunoglobulin complex and plasma membrane signaling receptor complex. The MF term was also related to immune response, such as antigen binding, immunoglobulin receptor binding and immune receptor activity. The results of KEGG analysis are shown in Figure 6B. Most genes were enriched in cytokine-cytokine receptor interaction, cell adhesion molecules and chemokine signaling pathway.

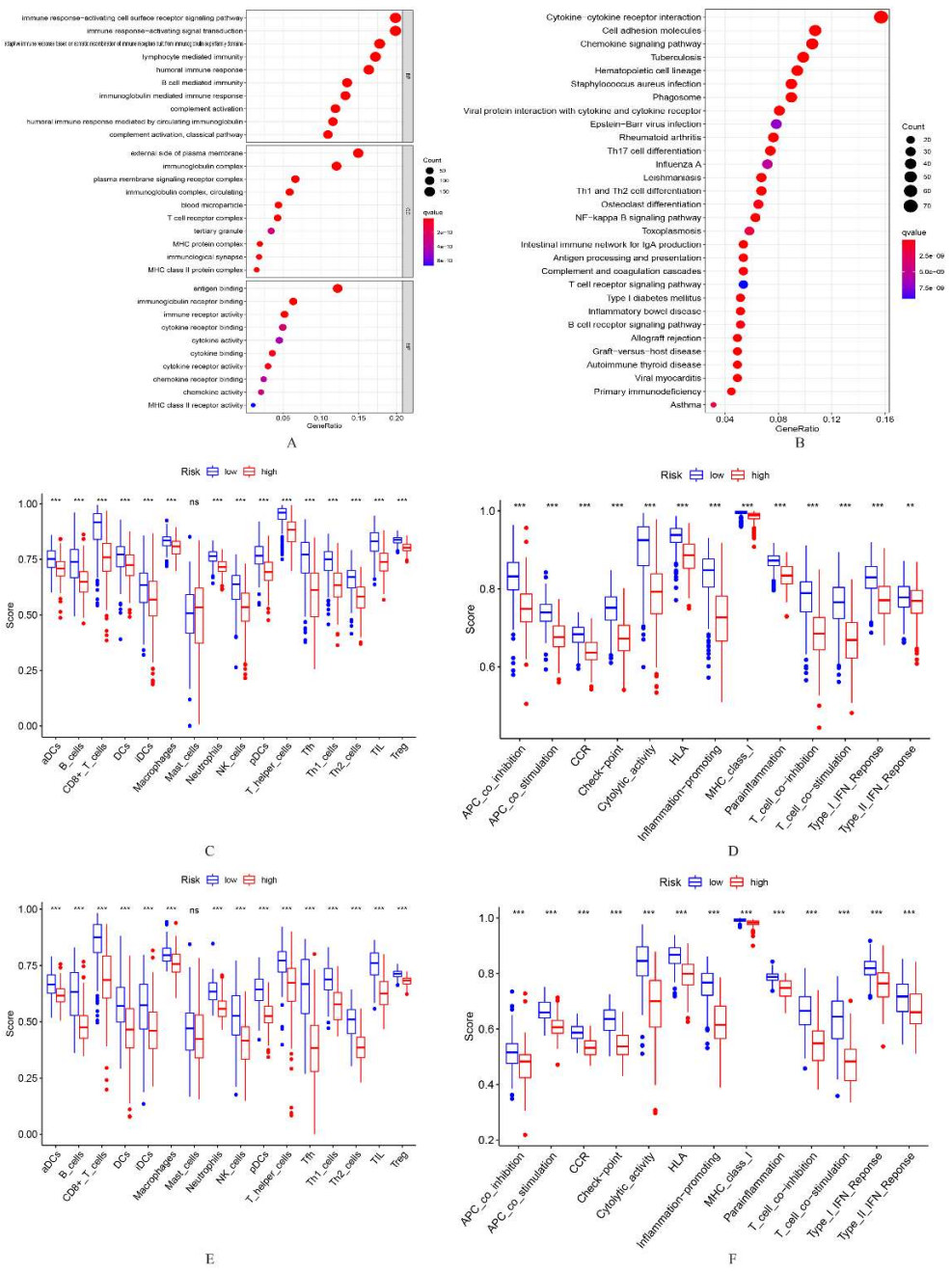

Figure 6. A. GO analysis of DEGs between high-risk and low-risk groups; B. KEGG analysis of DEGs between high-risk and low-risk groups; C, D. Comparison of the enrichment scores of 16 types of immune cells and 13 immune-related pathways between low- and high-risk group in the entire TCGA cohort. E, F. Comparison of the enrichment scores of 16 types of immune cells and 13 immune-related pathways between low- and high-risk group in the external validation cohort (GSE65904).

Comparisons of the immune activity between the two groups in the entire TCGA cohort are shown in Figure 6C,D. Except mast cells, almost all the other types of cells were highly infiltrated in the low-risk group (all P value < 0.001). All immune pathways were significantly up-regulated in the low-risk group. Similar conclusions were drawn in the external validation group (Figure 6E,F).

3.6. Patient response to immune checkpoint inhibitors

Patient response to immune therapies was evaluated by immunophenoscore. As shown in Figure 7A-D, the IPS-PD1, IPS-CTL4 and IPS-PD1 and CTL4 were significantly higher in the low risk score group. Meanwhile, we evaluated the expression pattern of PD-1 (PDCD1), PD-L1 (CD274), PD-L2 (PDCD1LG2) and CTLA4 in melanoma patients. Unsurprisingly, both of them were highly expressed in the low risk score group (Figures 7E-H). These results indicated that patients with low risk score had a better opportunity for immune checkpoint inhibitors therapy.

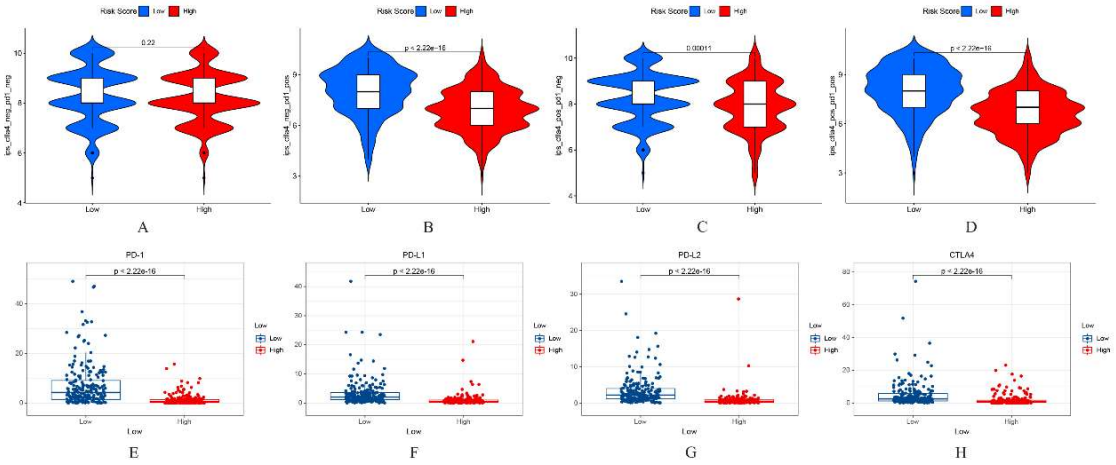

Figure 7. Patient response to immune checkpoint inhibitors. A. there were no differences between two groups if PD-1 and CLAT-4 were all negatively expressed. B-D. patients in low risk score group were prone to immune check point inhibitors if either PD-1 and CLAT-4 were positively expressed. E-H. The expressions of PD-1, PD-L1, PD-L2 and CTLA were significantly higher in the low risk score group ($P < 0.001$).

4. Discussion

In this study, we began by identifying differently expressed pyroptosis-related genes. Then, prognosis values of each gene were accessed by univariate Cox regression analysis. Intersected genes were included to perform LASSO regression analysis and multivariate Cox regression analysis to build a prognostic model in the training cohort. This model was further validated in the internal validation cohort and external validation cohort. The functional analyses showed that most DEGs were enriched in immune-related pathways. Immune cell infiltration and immune-related pathway analysis showed that the low-risk group had increased levels of infiltrating immune cells and increased activation of immune-related pathways. Patient response to immune therapies was evaluated and the results showed that patients with low risk score had a better opportunity for immune checkpoint inhibitors therapy.

Recently, molecular biomarkers have provided some insights into the prognosis-predicting process. A large number of genes have been proven to have prognostic potential. For example, higher expressions of Cytoplasmic Pin1 (Pin1) [19], Cell division cycle associated 8 (CDCA8) [20] and T-Box Transcription Factor Protein 21 (TBX21) [21] were believed to be related to poorer prognosis in SKCM. However, prognostic models based on single gene expression usually have low reliability. Thus, models based on specific features and biological functions, such as immune response [22] and

metastasis [23], have become a hot spot in the process of predicting patients' survival. These models also further illustrated several underlying mechanisms of SKCM at the same time. In this study, we constructed a novel model based on pyroptosis-related genes which have not been fully illustrated in SKCM.

Pyroptosis is a form of programmed cell death (PCD), which is triggered by the activation of inflammasomes [24,25]. Inflammasomes were reported to have wide connections with defense of cells against infections, cell death, obesity and cancers [26]. Generally, inflammasomes contain an adaptor protein apoptosis-associated speck-like protein which is binding to caspase-1 and sensors which could recognize cell injury products. The sensors could be categorized into nucleotide−binding domain-like receptors (NLRs) and absent in melanoma 2 (AIM2)-like receptors (ALRs). Downstream of activating inflammasomes is activating caspase-1, IL-1β, IL-18 and cleaving proteins of gasdermin family, thus, result in the activation of pyroptosis [27]. During these years, the importance of inflammasomes in melanoma progression and treatment have been well illustrated. Al Emran et al. [25] compared the expression pattern of several inflammasome mediators and found that low expression of inflammasome mediators is associated with poor prognosis in melanoma. Segovia et al. [28] found that targeting transmembrane protein 176B could enhance the efficacy of immune checkpoint blockers by unleashing inflammasome activation. Ahmed et al. [29] reported that BRAFi resistant melanoma lines can be killed by activators of AIM2 and NLRP3 inflammasomes.

Pyroptosis bears some similarity with apoptosis (another form of PCD) such as DNA damage, nuclear condensation and caspase independence [30]. It also has some distinctive morphological features [5,24,31]. Firstly, membranes of pyroptostic cells remain intact while their DNAs have been fragmented. Therefore, these cells are positive to TUNEL staining. Secondly, inflammation-induced pore formation results in cell swelling and osmotic lysis. It seems that pyroptosis serves as a double-edged sword in tumor formation [5]. On one hand, leakage of cell contains is responsible for the inflammation microenvironment which is a promoter for tumor genesis [32]. On the other hand, as a form of PCD, pyroptosis can inhibit tumor formation and proliferation [33]. Given the role of pyroptosis in tumor, Ye et al. [13] built a prognostic model in ovarian cancer based on 34 pyroptosis-related genes. Unlike their findings, we found pyroptosis may be more critical to SKCM. Firstly, as shown in Figure 2B, almost all intersected genes were closely related to SKCM prognosis (threshold was set as $P < 0.05$). Secondly, the AUC of our model was 0.664 at 1 year, 0.666 at 2 years and 0.641 at 3 years. All of them were higher than in the model of ovarian cancer.

There were four genes included in the model, namely GSDMA, GSDMC, AIM2 and NOD2. GSDMA belongs to gasdermins protein family (GSDM), which is a group of pore-forming proteins [34]. In 2016, Ding et al. [35] reported the crystal structure of full length GSDMA. It adopts an auto-inhibited conformation, which means that the N-terminal domain is inhibited by the C-terminal domain. GSDMA functions as a pore-forming protein and is associated with the formation of oligomer on the membrane surface, known as the "pre-pore stage" in pyroptosis [36]. In humans, GSDMA is expressed in the esophagus, lower gastrointestinal tract, mammary gland and skin [37]. As indicated by Saeki et al. [38], it was a cell-growth inhibitor in gastric cancers (GC). However, some researchers [5] also reported that GSDMA was not expressed in normal colorectal epithelial cells and overexerted in carcinoma cells. In this study, we found an intriguing outcome related to the function of GSDMA in SKCM. Although it was down-regulated in melanoma samples, Cox regression analyses showed that the lower expression of GSDMA was associated with better survival states. This might have occurred for two reasons. Firstly, the expression of GSDMA might be affected by several factors, such as the cancer microenvironment,

inflammatory and immune cell infiltration. Secondly, DEGs were filtered by combining TCGA and GTEx database for lack of normal samples. Given the limited data, the function of GSDMA still needs to be further studied. GSDMC, also known as MLZE, is isolated by Watabe et al. [39] It is also a member of GSDM family. In humans, GSDMC is expressed in the trachea, spleen and metastatic melanoma cells [39]. Hou et al. [40] noted that higher expression of GSDMC was correlated with poorer survival in breast cancer. The oncogene property of GSDMC was also noted in lung adenocarcinoma and colorectal cancer [41,42]. The function of GSDMC in tumors has been controversial because it is also down regulated in many esophageal and gastric cancer cells [38]. In this study, we found that higher expression of GSDMC was associated with poorer survival states, which is similar to Ito et al. [43] and Watabe et al. [39]. The mechanism by which GSDMC was down-regulated in tumor samples remains to be elucidated. Full name of AIM2 is absent in melanoma 2. It works as a cytosolic innate immune receptor by recognizing double-stranded DNA (dsDNA) released during cellular perturbation and pathogenic assault [44]. After recognition of dsDNA, AIM2 could lead the formation of inflammasome and induce pyroptosis. It is well illustrated that AIM2 played a double role in tumor formation and proliferation. Xu et al. [45] reported that AIM2 could inhibit colorectal cancer cell proliferation and migration. In contrast, Martínez-Cardona et al. reported that AIM2 deficiency reduced the development of hepatocellular carcinoma (HCC). Tumor promotion properties of AIM2 were also found in cutaneous squamous cell carcinoma [46]. In this study, we found that AIM2 was highly expressed however it was recognized as a protective factor in univariate Cox regression analysis. We speculated that this inconsistence was caused by the complex expression regulation. The role of AIM2 in melanoma patients still need further explorations. NOD2 is a member of intracellular NOD-like receptor family, which senses conserved motifs in bacterial peptidoglycan and induces pro-inflammatory and anti-microbial responses [47]. So far, the role of NOD2 in tumor formation has not been fully illustrated. NOD2 could serve as a protective factor in hepatocellular carcinoma [48,49]. However, Zhou et al. [50]. illustrated that hepatic NOD2 could promote hepatocarcinogenesis. NOD2 seems to be a tumor suppressor in melanoma. Fujimura et al. [51] reported that a synthetic NOD2 agonist could suppress melanoma growth. Our findings are similar to Fujimura et al. we also found NOD2 was down regulated in tumor samples and positively related to patients' survival. Although the prognostic model based on these four genes has achieved fair outcomes in training and validation groups, we still found some controversial findings in this study. We speculated that these contradictions are inevitable because the underlying mechanism and interactions between these genes are largely unknown. Further in-depth studies are still needed.

In this study, we divided patients into the high-risk and low-risk group and found that the differences between the two groups are mainly enriched in immune-related pathways. Surprisingly, we also found the levels of key antitumor infiltrating immune cells were higher in the low-risk group. Previous studies have proven that high infiltration of T cells, B cells and NK cells was a good prognosis factor for SKCM survival [52−54]. Except for the type II IFN response pathway, other immune pathways were highly activated in the low-risk group. These findings indicated that pyroptosis might inhibit tumor malignance by activating immune response, which is similar to Zhang et al. [55] and Wang et al. [56] These two studies reported that tumor cells undergoing pyroptosis recruit tumor suppressed immune cells. Wang et al. [56] revealed that less than 15% tumor cell pyroptosis could clear entire grafted tumor in vivo studies. Another study conducted by Zhang et al. [55] indicated that $CD8^+$ T cells and NK cells were infiltrated in a pyroptosis-activated immune microenvironment. In turn, $CD8^+$ T cells and NK cells could induce tumor cell pyroptosis and form a positive feedback loop.

Pyroptosis could affect the efficacy of immune checkpoint inhibitors (ICIs) therapies. ICIs were a landscape of metastasis melanoma and significantly improved patients' survival. However, there are still patients who are resistant to ICIs, which was known as "cold" [57]. Wang et al. [56] reported that combined use of ICIs and pyroptosis inducers could effectively kill these "cold" cells. Currently, drugs targeted enhancing pyroptosis and immune response have shown great potential in tumor therapy. For example, Zhang et al. [58] reported that paclitaxel could induce pyroptosis by activating caspase-3/GSDME in lung cancer cells. Yue et al. [59] reported that anthocyanin could induce pyroptosis in oral squamous cell carcinoma. These pyroptosis inducers were also used in SKCM therapy [60−62]. The underlying mechanisms need to be further studied to provide more effective therapies for patients. Several biomarkers, including PD-1 CTLA-4 and T cell exhaustion genes could be used to predict the response to ICBs. PD-1 is one the critical checkpoint in T cells and B cells. After engagement with its ligands PD-L1 or PD-L2, PD-1 is activated, leading to the inhibition of T cell proliferation, activation and cytokine production [63]. Kleffel et al. [64] reported that melanoma cell-intrinsic PD-1 could promote tumor growth whereas PD-L1 inhibition or knockout of host-PD-L1 could attenuate growth of melanoma cells. CTLA-4 is also an inhibitor of T cell activation by binding to CD80 or CD86 on the surface of antigen-presenting cells (APCs) [65]. In 2010, ipilimumab (CTLA-4 blocker) [66] was approved for the treatment of advanced melanoma. Since then, numerous ICBs have been tested in clinical trials [67]. In this study, we found PD-1, PD-L1, PD-L2 and CTLA-4 were highly expressed in the low risk score group. Correspondingly, they are more sensitive to PD-1 blocker, CTLA-4 blocker and PD-1 and CTLA-4 blocker as indicated by immunophenoscore.

Undeniably, our studies shave several limitations. Firstly, this model was established based on TCGA training database and validated in one internal cohort and one external cohort. Consequently, high quality external validation cohorts are needed to test these findings. Secondly, the mechanisms of pyroptosis in SKCM need to be further explored. Even with these limitations, our study had several potential implications in patients' survival prediction.

5. Conclusions

In conclusion, our study demonstrated that pyroptosis was closely related to SKCM. Almost all pyroptosis related genes were differently expressed between SKCM and normal tissues. The risk score based on this model could serve as an independent prognosis-predicting factor. DEGs between high-risk and low-risk groups were mainly enriched in immune-related pathways and more immune cells were infiltrated in low-risk group patients. In addition, patients with low risk score had a better opportunity for immune checkpoint inhibitors therapy. Our study provided an insight into the function and prognostic value of pyroptosis in SKCM.

Conflict of interest

The authors declare no competing interests

References

1. R. L. Siegel, K. D. Miller, H. E. Fuchs, A. Jemal, Cancer statistics, *CA Cancer J. Clin.*, **71** (2021), 7−33. doi: 10.3322/caac.20073.

2. K. D. Miller, L. Nogueira, A. B. Mariotto, J. H. Rowland, K. R. Yabroff, C. M. Alfano, et al., Cancer treatment and survivorship statistics, *CA Cancer J. Clin.*, **69** (2019), 363−385. doi: 10.3322/caac.21235.
3. R. R. Kudchadkar, M. C. Lowe, M. K. Khan, S. M. McBrien, Metastatic melanoma, *CA Cancer J. Clin.*, **70** (2020), 78−85. doi: 10.3322/caac.21599.
4. M. Rastrelli, S. Tropea, C. R. Rossi, M. Alaibac, Melanoma: epidemiology, risk factors, pathogenesis, diagnosis and classification, *In Vivo*, **28** (2014), 1005−1011.
5. X. Xia, X. Wang, Z. Cheng, W. Qin, L. Lei, J. Jiang, et al., The role of pyroptosis in cancer: pro-cancer or pro-"host"?, *Cell Death Dis.*, **10** (2019), 650. doi: 10.1038/s41419-019-1883-8.
6. P. Yu, H. Y. Wang, M. Tian, A. X. Li, X. S. Chen, X. L. Wang, et al., Eukaryotic elongation factor-2 kinase regulates the cross-talk between autophagy and pyroptosis in doxorubicin-treated human melanoma cells in vitro, *Acta Pharmacol. Sin.*, **40** (2019), 1237−1244. doi: 10.1038/s41401-019-0222-z.
7. S. Feng, D. Fox, S. M. Man, Mechanisms of gasdermin family members in inflammasome signaling and cell death, *J. Mol. Biol.*, **430** (2018), 3068−3080. doi: 10.1016/j.jmb.2018.07.002.
8. C. Lee, H. T. T. Do, J. Her, Y. Kim, D. Seo, I. Rhee, Inflammasome as a promising therapeutic target for cancer, *Life Sci.*, **231** (2019), 116593. doi: 10.1016/j.lfs.2019.116593.
9. W. Hong, Y. Gu, R. Guan, D. Xie, H. Zhou, M. Yu, Pan-cancer analysis of the CASP gene family in relation to survival, tumor-infiltrating immune cells and therapeutic targets, *Genomics*, **112** (2020), 4304−4315. doi: 10.1016/j.ygeno.2020.07.026.
10. Q. Wei, K. Mu, T. Li, Y. Zhang, Z. Yang, X. Jia, et al., Deregulation of the NLRP3 inflammasome in hepatic parenchymal cells during liver cancer progression, *Lab Invest.*, **94** (2014), 52−62. doi: 10.1038/labinvest.2013.126.
11. M. Hergueta-Redondo, D. Sarrió, Á Molina-Crespo, D. Megias, A. Mota, A. Rojo-Sebastian, et al., Gasdermin-B promotes invasion and metastasis in breast cancer cells, *PLoS One*, **9** (2014), e90099. doi: 10.1371/journal.pone.0090099.
12. W. J. Wang, D. Chen, M. Z. Jiang, B. Xu, X. W. Li, Y. Chu, et al., Downregulation of gasdermin D promotes gastric cancer proliferation by regulating cell cycle-related proteins, *J. Dig. Dis.*, **19** (2018), 74−83. doi: 10.1111/1751-2980.12576.
13. Y. Ye, Q. J. Dai, H. B. Qi, A novel defined pyroptosis-related gene signature for predicting the prognosis of ovarian cancer, *Cell Death Discov.*, **7** (2021), 71. doi: 10.1038/s41420-021-00451-x.
14. D. A. Erkes, W. Cai, I. M. Sanchez, T. J. Purwin, C. Rogers, C. O. Field, et al., Mutant BRAF and MEK inhibitors regulate the tumor immune microenvironment via pyroptosis, *Cancer Discov.*, **10** (2020), 254−269. doi: 10.1158/2159-8290.CD-19-0672.
15. B. Zhou, J. Y. Zhang, X. S. Liu, H. Z. Chen, Y. L. Ai, K. Cheng, et al., Tom20 senses iron-activated ROS signaling to promote melanoma cell pyroptosis, *Cell Res.*, **28** (2018), 1171−1185. doi: 10.1038/s41422-018-0090-y.
16. J. Long, L. Zhang, X. Wan, J. Lin, Y. Bai, W. Xu, et al., A four-gene-based prognostic model predicts overall survival in patients with hepatocellular carcinoma, *J. Cell Mol. Med.*, **22** (2018), 5928−5938. doi: 10.1111/jcmm.13863.
17. Y. Jia, Y. Chen, J. Liu, Prognosis-predictive signature and nomogram based on autophagy-related long non-coding RNAs for hepatocellular carcinoma, *Front. Genet.*, **11** (2020), 608668. doi: 10.3389/fgene.2020.608668.

18. P. Charoentong, F. Finotello, M. Angelova, C. Mayer, M. Efremova, D. Rieder, et al., Pan-cancer immunogenomic analyses reveal genotype-immunophenotype relationships and predictors of response to checkpoint blockade, *Cell Rep.*, **18** (2017), 248−262. doi: 10.1016/j.celrep.2016.12.019.
19. D. Yan, S. Hu, Z. Zhou, S. Zeenat, F. Cheng, Y. Li, et al., Different chemical groups modification on the surface of chitosan nonwoven dressing and the hemostatic properties, *Int. J. Biol. Macromol.*, **107** (2018), 463−469. doi: 10.1016/j.ijbiomac.2017.09.008.
20. C. Ci, B. Tang, D. Lyu, W. Liu, D. Qiang, X. Ji, et al., Overexpression of CDCA8 promotes the malignant progression of cutaneous melanoma and leads to poor prognosis, *Int. J. Mol. Med.*, **43** (2019), 404−412. doi: 10.3892/ijmm.2018.3985.
21. X. Zhang, X. Wen, N. Feng, A. Chen, S. Yao, X. Ding, et al., Increased expression of T-Box transcription factor protein 21 (TBX21) in skin cutaneous melanoma predicts better prognosis: A study based on The Cancer Genome Atlas (TCGA) and Genotype-Tissue Expression (GTEx) databases, *Med. Sci. Monit.*, **26** (2020), e923087. doi: 10.12659/MSM.923087.
22. B. Huang, W. Han, Z. F. Sheng, G. L. Shen, Identification of immune-related biomarkers associated with tumorigenesis and prognosis in cutaneous melanoma patients, *Cancer Cell Int.*, **20** (2020), 195. doi: 10.21203/rs.2.23305/v3.
23. Q. Wan, C. Liu, C. Liu, W. Liu, X. Wang, Z. Wang, Discovery and validation of a metastasis-related prognostic and diagnostic biomarker for melanoma based on single cell and gene expression datasets, *Front. Oncol.*, **10** (2020), 585980. doi: 10.3389/fonc.2020.585980.
24. Y. Fang, S. Tian, Y. Pan, W. Li, Q. Wang, Y. Tang, et al., Pyroptosis: A new frontier in cancer, *Biomed. Pharmacother.*, **121** (2020), 109595. doi: 10.1016/j.biopha.2019.109595.
25. A. A. Emran, H. Y. Tseng, M. C. Coleman, J. Tiffen, S. Cook, H. M. McGuire, et al., Do innate killing mechanisms activated by inflammasomes have a role in treating melanoma?, *Pigment Cell Melanoma Res.*, **33** (2020), 660−670. doi: 10.1111/pcmr.12870.
26. H. Guo, J. B. Callaway, J. P. Ting, Inflammasomes: mechanism of action, role in disease, and therapeutics, *Nat. Med.*, **21** (2015), 677−687. doi: 10.1038/nm.3893.
27. C. Rogers, D. A. Erkes, A. Nardone, A. E. Aplin, T. Fernandes-Alnemri, E. S. Alnemri, Gasdermin pores permeabilize mitochondria to augment caspase-3 activation during apoptosis and inflammasome activation, *Nat. Commun.*, **10** (2019), 1689. doi: 10.1038/s41467-019-09397-2.
28. M. Segovia, S. Russo, M. Jeldres, Y. D. Mahmoud, V. Perez, M. Duhalde, et al., Targeting TMEM176B enhances antitumor immunity and augments the efficacy of immune checkpoint blockers by unleashing inflammasome activation, *Cancer Cell*, **35** (2019), 767−781. e766. doi: 10.1016/j.ccell.2019.04.003.
29. F. Ahmed, H. Y. Tseng, A. Ahn, D. Gunatilake, S. Alavi, M. Eccles, et al., Repurposing melanoma chemotherapy to activate inflammasomes in treatment of BRAF/MAPK inhibitor resistant melanoma, *J. Invest. Dermatol.*, **2021** (2021). doi: 10.1016/j.jid.2021.09.030.
30. Y. Tan, Q. Chen, X. Li, Z. Zeng, W. Xiong, G. Li, et al., Correction to: Pyroptosis: a new paradigm of cell death for fighting against cancer, *J. Exp. Clin. Cancer Res.*, **40** (2021), 219. doi: 10.1186/s13046-021-01959-x.
31. J. Yu, Q. Wang, X. Zhang, Z. Guo, X. Cui, Mechanisms of neoantigen-targeted induction of pyroptosis and ferroptosis: From basic research to clinical applications, *Front. Oncol.*, **11** (2021), 685377. doi: 10.3389/fonc.2021.685377.

32. L. M. Coussens, Z. Werb, Inflammation and cancer, *Nature*, **420** (2002), 860−867. doi: 10.1186/s12199-018-0740-1.
33. K. Nagarajan, K. Soundarapandian, R. F. Thorne, D. Li, D. Li, Activation of pyroptotic cell death pathways in cancer: An alternative therapeutic approach, *Transl. Oncol.*, **12** (2019), 925−931. doi: 10.1016/j.tranon.2019.04.010.
34. C. Berkel, E. Cacan, Differential expression and Copy Number Variation of Gasdermin (GSDM) family members, pore-forming proteins in pyroptosis, in normal and malignant serous ovarian tissue, *Inflammation*, **2021** (2021). doi: 10.1007/s10753-021-01493-0.
35. J. Ding, K. Wang, W. Liu, Y. She, Q. Sun, J. Shi, et al., Pore-forming activity and structural autoinhibition of the gasdermin family, *Nature*, **535** (2016), 111−116. doi: 10.1038/nature18590.
36. J. Ruan, S. Xia, X. Liu, J. Lieberman, H. Wu, Cryo-EM structure of the gasdermin A3 membrane pore, *Nature*, **557** (2018), 62−67. doi: 10.1038/s41586-018-0058-6.
37. N. Saeki, Y. Kuwahara, H. Sasaki, H. Satoh, T. Shiroishi, Gasdermin (Gsdm) localizing to mouse Chromosome 11 is predominantly expressed in upper gastrointestinal tract but significantly suppressed in human gastric cancer cells, *Mamm. Genome.*, **11** (2000), 718−724. doi: 10.1007/s003350010138.
38. N. Saeki, T. Usui, K. Aoyagi, D. H. Kim, M. Sato, T. Mabuchi, et al., Distinctive expression and function of four GSDM family genes (GSDMA-D) in normal and malignant upper gastrointestinal epithelium, *Genes Chromosomes Cancer*, **48** (2009), 261−271. doi: 10.1002/gcc.20636.
39. K. Watabe, A. Ito, H. Asada, Y. Endo, T. Kobayashi, K. Nakamoto, et al., Structure, expression and chromosome mapping of MLZE, a novel gene which is preferentially expressed in metastatic melanoma cells, *Jpn. J. Cancer Res.*, **92** (2001), 140−151. doi: 10.1111/j.1349-7006.2001.tb01076.x.
40. J. Hou, R. Zhao, W. Xia, C. W. Chang, Y. You, J. M. Hsu, et al., PD-L1-mediated gasdermin C expression switches apoptosis to pyroptosis in cancer cells and facilitates tumour necrosis, *Nat. Cell Biol.*, **22** (2020), 1264−1275. doi: 10.1038/s41556-020-0575-z.
41. M. Miguchi, T. Hinoi, M. Shimomura, T. Adachi, Y. Saito, H. Niitsu, et al., Gasdermin C Is upregulated by inactivation of transforming growth factor β receptor Type II in the presence of mutated apc, promoting colorectal cancer proliferation, *PLoS One*, **11** (2016), e0166422. doi: 10.1371/journal.pone.0166422.
42. J. Wei, Z. Xu, X. Chen, X. Wang, S. Zeng, L. Qian, et al., Overexpression of GSDMC is a prognostic factor for predicting a poor outcome in lung adenocarcinoma, *Mol. Med. Rep.*, **21** (2020), 360−370. doi: 10.3892/mmr.2019.10837.
43. A. Ito, K. Watabe, Y. Koma, Y. Kitamura, An attempt to isolate genes responsible for spontaneous and experimental metastasis in the mouse model, *Histol. Histopathol.*, **17** (2002), 951−959. doi: 10.14670/HH-17.951.
44. B. R. Sharma, R. Karki, T. D. Kanneganti, Role of AIM2 inflammasome in inflammatory diseases, cancer and infection, *Eur. J. Immunol.*, **49** (2019), 1998−2011. doi: 10.1002/eji.201848070.
45. M. Xu, J. Wang, H. Li, Z. Zhang, Z. Cheng, AIM2 inhibits colorectal cancer cell proliferation and migration through suppression of Gli1, *Aging (Albany NY)*, **13** (2020), 1017−1031. doi: 10.18632/aging.202226.
46. M. Farshchian, L. Nissinen, E. Siljamäki, P. Riihilä, M. Piipponen, A. Kivisaari, et al., Tumor cell-specific AIM2 regulates growth and invasion of cutaneous squamous cell carcinoma, *Oncotarget*, **8** (2017), 45825−45836. doi: 10.18632/oncotarget.17573.

47. R. Caruso, N. Warner, N. Inohara, G. Núñez, NOD1 and NOD2: signaling, host defense, and inflammatory disease, *Immunity*, **41** (2014), 898−908. doi: 10.1016/j.immuni.2014.12.010.
48. X. Ma, Y. Qiu, Y. Sun, L. Zhu, Y. Zhao, T. Li, et al., NOD2 inhibits tumorigenesis and increases chemosensitivity of hepatocellular carcinoma by targeting AMPK pathway, *Cell Death Dis.*, **11** (2020), 174. doi: 10.1038/s41419-020-2368-5.
49. S. A. Gurses, S. Banskar, C. Stewart, B. Trimoski, R. Dziarski, D. Gupta, Nod2 protects mice from inflammation and obesity-dependent liver cancer, *Sci. Rep.*, **10** (2020), 20519. doi: 10.1038/s41598-020-77463-7.
50. Y. Zhou, L. Hu, W. Tang, D. Li, L. Ma, H. Liu, et al., Hepatic NOD2 promotes hepatocarcinogenesis via a RIP2-mediated proinflammatory response and a novel nuclear autophagy-mediated DNA damage mechanism, *J. Hematol. Oncol.*, **14** (2021), 9. doi: 10.1186/s13045-020-01028-4.
51. T. Fujimura, K. Yamasaki, T. Hidaka, Y. Ito, S. Aiba, A synthetic NOD2 agonist, muramyl dipeptide (MDP)-Lys (L18) and IFN-β synergistically induce dendritic cell maturation with augmented IL-12 production and suppress melanoma growth, *J. Dermatol. Sci.*, **62** (2011), 107−115. doi: 10.1016/j.jdermsci.2011.02.002.
52. A. Ladányi, Prognostic and predictive significance of immune cells infiltrating cutaneous melanoma, *Pigment Cell Melanoma Res.*, **28** (2015), 490−500. doi: 10.1111/pcmr.12371.
53. S. R. Selitsky, L. E. Mose, C. C. Smith, S. Chai, K. A. Hoadley, D. P. Dittmer, et al., Prognostic value of B cells in cutaneous melanoma, *Genome Med.*, **11** (2019), 36. doi: 10.1186/s13073-019-0647-5.
54. M. Tucci, A. Passarelli, F. Mannavola, C. Felici, L. S. Stucci, M. Cives, et al., Immune system evasion as hallmark of melanoma progression: The role of dendritic cells, *Front. Oncol.*, **9** (2019), 1148. doi: 10.3389/fonc.2019.01148.
55. Z. Zhang, Y. Zhang, S. Xia, Q. Kong, S. Li, X. Liu, et al., Gasdermin E suppresses tumour growth by activating anti-tumour immunity, *Nature*, **579** (2020), 415−420. doi: 10.1038/s41586-020-2071-9.
56. Q. Wang, Y. Wang, J. Ding, C. Wang, X. Zhou, W. Gao, et al., A bioorthogonal system reveals antitumour immune function of pyroptosis, *Nature*, **579** (2020), 421−426. doi: 10.1038/s41586-020-2079-1.
57. S. L. Topalian, J. M. Taube, R. A. Anders, D. M. Pardoll, Mechanism-driven biomarkers to guide immune checkpoint blockade in cancer therapy, *Nat. Rev. Cancer*, **16** (2016), 275−287. doi: 10.1038/nrc.2016.36.
58. C. C. Zhang, C. G. Li, Y. F. Wang, L. H. Xu, X. H. He, Q. Z. Zeng, et al., Chemotherapeutic paclitaxel and cisplatin differentially induce pyroptosis in A549 lung cancer cells via caspase−3/GSDME activation, *Apoptosis*, **24** (2019), 312−325. doi: 10.1007/s10495-019-01515-1.
59. E. Yue, G. Tuguzbaeva, X. Chen, Y. Qin, A. Li, X. Sun, et al., Anthocyanin is involved in the activation of pyroptosis in oral squamous cell carcinoma, *Phytomedicine*, **56** (2019), 286−294. doi: 10.1016/j.phymed.2018.09.223.
60. R. Ghiman, M. Nistor, M. Focșan, A. Pintea, S. Aștilean, D. Rugina, Fluorescent polyelectrolyte system to track anthocyanins delivery inside melanoma cells, *Nanomaterials (Basel)*, **11** (2021), 782. doi: 10.3390/nano11030782.

61. A. Ashworth, ATR inhibitors and paclitaxel in melanoma, *Clin. Cancer Res.*, **27** (2021), 4667−4668. doi: 10.1158/1078-0432.CCR-21-1778.
62. J. J. Li, J. H. Wang, Y. Dingv, D. D. Li, X. Z. Wen, J. J. Zhao, et al., Efficacy and safety of anti-PD-1 inhibitor combined with nab-paclitaxel in Chinese patients with refractory melanoma, *J. Cancer Res. Clin. Oncol.*, **2021** (2021). doi: 10.1007/s00432-021-03700-9.
63. L. Ai, A. Xu, J. Xu, Roles of PD-1/PD-L1 pathway: Signaling, cancer, and beyond, *Adv. Exp. Med. Biol.*, **1248** (2020), 33−59. doi: 10.1007/978-981-15-3266-5_3.
64. S. Kleffel, C. Posch, S. R. Barthel, H. Mueller, C. Schlapbach, E. Guenova, et al., Melanoma cell-intrinsic PD-1 receptor functions promote tumor growth, *Cell*, **162** (2015), 1242−1256. doi: 10.1016/j.cell.2015.08.052.
65. B. Rowshanravan, N. Halliday, D. M. Sansom, CTLA-4: a moving target in immunotherapy, *Blood*, **131** (2018), 58−67. doi: 10.1182/blood-2017-06-741033.
66. F. S. Hodi, S. J. O'Day, D. F. McDermott, R. W. Weber, J. A. Sosman, J. B. Haanen, et al., Improved survival with ipilimumab in patients with metastatic melanoma, *N. Engl. J. Med.*, **363** (2010), 711−723. doi: 10.1056/NEJMoa1003466.
67. T. N. Gide, J. S. Wilmott, R. A. Scolyer, G. V. Long, Primary and acquired resistance to immune checkpoint inhibitors in metastatic melanoma, *Clin. Cancer Res.*, **24** (2018), 1260−1270. doi: 10.1016/j.jtho.2021.01.131.

AIMS Press